Research Article

Ternary Ag nanoparticles/natural-magnetic SiO_2-nanowires/reduced graphene oxide nanocomposites with highly visible photocatalytic activity for 4-nitrophenol reduction

Xin Chen[1] · Jia Lei[1] · Yongpeng Wang[3] · Wenkun Zhu[1] · Weitang Yao[1] · Tao Duan[1,2]

Abstract
Agglomerate and reuse limit the promising application of silver nanoparticles (AgNPs) as catalyst. To eliminate those disadvantages, herein, Fe-containing silica nanowires (SiO_2NWs) and reduced graphene oxide (RGO) are used as suitable substrates to prepare AgNPs/SiO_2NWs/RGO nanocomposite via self-assembly approach. The nanocomposite mostly assembled with each other via intermolecular hydrogen bond and electrostatic adsorption to form a three-dimensional network structure. The AgNPs/SiO_2NWs/RGO nanocomposite exhibit excellent photocatalytic activity for 4-nitrophenol reduction by $NaBH_4$, originating from that the nearly mono-dispersed AgNPs are adhered on the surface of the SiO_2NWs and RGO, allowing the effective contact of reactants with catalyst and facilitating the electron transfer between them in the reaction. The obtained nanocomposites exhibit the superior stability and can be easily recovered with their fully catalytic activities due to the hydrophobic and magnetic properties of the nanocomposites. It shows the great prospect for the 4-NP reduction in practice and is promising for wide applications in visible light catalytic reaction.

Keywords Reduced graphene oxide · SiO_2 nanowires · Silver nanoparticles · 4-Nitrophnol reduction · Photo-catalytic activity

1 Introduction

Due to the outstanding catalytic properties of silver nanoparticles (AgNPs), it was considered as one of the most promising functional materials in the field of electronics, chemicals, biologics and catalyst for a long time [1–3]. However, agglomerate and reuse were the main drawbacks for limiting its application. To solve the disadvantage of AgNPs, traditional strategies of dispersed AgNPs on a suitable substrate were used to form hybrid catalysts by chemical synthesis methods (such as polymers, metal oxides, silica nanotubes, carbon nanofibers, etc.) [4–8]. Silica nanomaterial was one of the suitable substrates because of material availability and environmental friendly [3, 7, 9–12]. In recent years, many silicon oxide nanostructures have been studied to assemble AgNPs via different methods include chemical plating [13–15], ultrasonication [16], in situ assembly and in situ reduction [12, 17, 18], electro static interaction [19] etc. Conventional methods, using silane and other organic reagent to prepare nano silicon dioxide, had a harmful effect on the environment in many previous studies, and also lack of sustainability. Therefore, it is necessary to develop a new synthesis method of nanometer silicon dioxide.

Electronic supplementary material The online version of this article (https://doi.org/10.1007/s42452-018-0124-6) contains supplementary material, which is available to authorized users.

✉ Tao Duan, duant@ustc.edu.cn | [1]Sichuan Co-Innovation Center for Energetic Materials, Southwest University of Science and Technology, Mianyang 621010, Sichuan, China. [2]Sichuan Civil-military Integration Institute, Mianyang 621010, Sichuan, China. [3]The Key Laboratory of Surface and Physical Chemistry, Chinese Academy of Engineering Physics, Jiangyou 621760, Sichuan, China.

SN Applied Sciences (2019) 1:130 | https://doi.org/10.1007/s42452-018-0124-6

Received: 12 October 2018 / Accepted: 12 December 2018 / Published online: 27 December 2018

Silica nanowires prepared from Chrysotile ($Mg_6[Si_4O_{10}](OH)_6$) was an excellent natural catalyst support candidate because of its outstanding physicochemical properties [12, 20, 21] and simple synthesis method [22]. As material sources are abundant and the reuse of Chrysotile asbestos tailings, the natural Chrysotile-based silica nanowires were comparatively cheap and became the better choice of catalyst support [12, 22]. In addition, the presence of associated mineral of Chrysotile made the prepared silica nanowires containing iron, which introduced the new property: magnetic property. Although various Ag/SiO_2 composites had effectively prevented the agglomerates of Ag NPs, the problem of the catalyst reuse still hadn't been solved very well due to the size of nanometer materials. It seems that the use of graphene could effectively solve this problem. As nanoscale silicon dioxide could be coated by graphene to form a hydrophobic composite [21], and graphene was another suitable holder which was studied due to its large surface area and unique optical, electronic, mechanical, catalytic properties in recent years [23–39]. To improve the catalytic property, these two suitable holders also were used together to combined with AgNPs [40, 41]. At the same time, it had great help for recyclable property.

Herein, we report a novel preparation process of synthesizing uniform three-dimensional network structure silver nanoparticles-silica nanowires-reduced graphene oxide ($AgNPs/SiO_2NWs/RGO$) nanocomposites (Scheme 1). Electrostatic adsorption between the three materials made it easy for AgNPs to adsorb on the surface of SiO_2NWs and RGO. Intermolecular hydrogen bond made the intense combination between SiO_2NWs and RGO. The motivations of this work are the developing of a facile solution strategy to prepare the large quantity and easily separable $AgNPs/SiO_2NWs/RGO$ nanocomposites, as well as to investigate their physical and chemical properties, nanostructures, and photocatalytic performance using the catalytic hydrogenation reduction of 4-nitrophenol to 4-aminophenol by sodium borohydride ($NaBH_4$) under visible light. This model reaction is commonly used to evaluate the catalytic performance of metal or metal oxide nanoparticles [26]. Particularly, 4-nitrophnol (4-NP) is the most toxic among the nitroaromatic compounds, one of priority pollutants listed by the United State Environmental Protection Agency (USEPA) due to its toxicity and durability [26, 31, 32, 39].

2 Experimental

2.1 Materials

Silicon dioxide nanowires (SiO_2NWs) [22], 3-aminopropyltriethoxysilane (γ-APS, 98%),acetic acid (CH_3COOH, 98%), silver nitrate ($AgNO_3$, 99.8%), sodium citrate ($C_6H_5Na_3O_7{\cdot}2H_2O$, 99%), and ethanol (EtOH, 99.7%) were supplied by Kelong Chemical Factory (Chengdu, China).

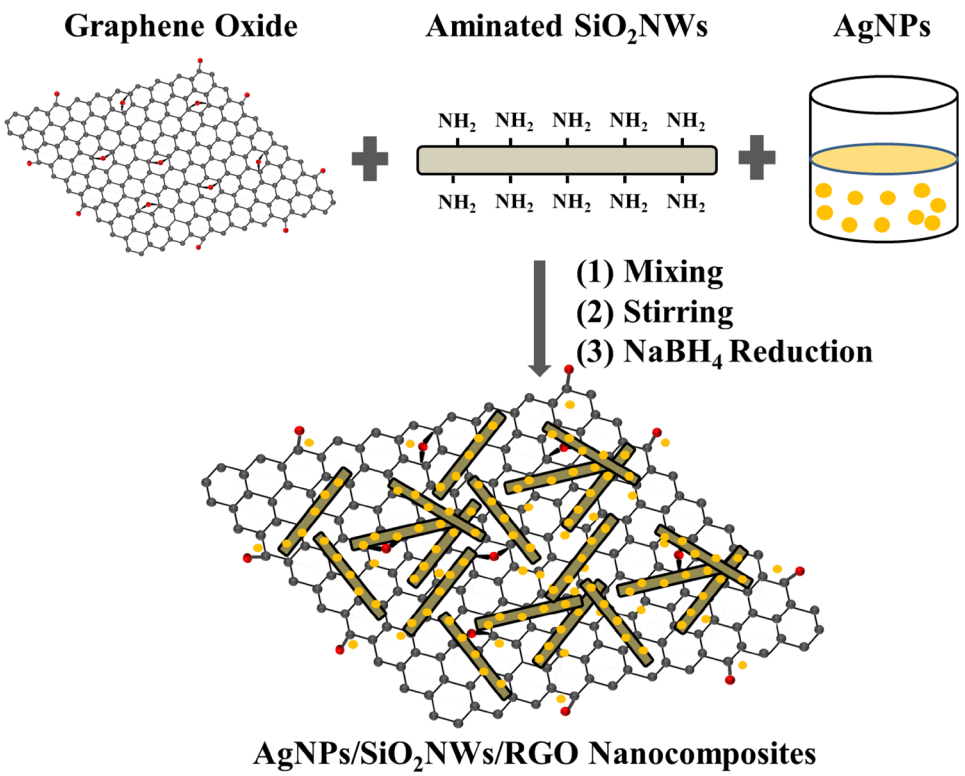

Scheme 1 Schematic diagram for preparation of $AgNPs/SiO_2NWs/RGO$ nanocomposites

Sodium borohydride ($NaBH_4$, 97%) and 4-nitrophenol ($C_6H_5NO_3$, 99.7%) were purchased from Aladin Ltd. (Shanghai, China). All chemicals were used without further purification. GO nanosheets were obtained from flake graphite (< 30 μm, Qingdao, China) by using the modified Hummers method [42]. The water used was purified through a Youpu system.

2.2 Preparation of AgNPs/SiO_2NWs/RGO nanocomposites

SiO_2NWs prepared from Chrysotile were aminated firstly by electron-rich 3-aminopropyltriethoxysilane. Procedure for amination was according to the method in Ref. [20]. 0.1 mg mL^{-1} of GO solution was prepared. GO nanosheets were obtained from flake graphite. The AgNPs were restored by sodium borohydride while electron-deficient sodium citrate acted as stabilizer. Typically, 25 mL of $AgNO_3$ (2 mmol L^{-1}) and 25 mL of sodium citrate (4 mmol L^{-1}) solution were mixed and stirred at 333 K for about 20 min. After addition of 0.6 mL of $NaBH_4$ (10 mmol L^{-1}), the mixed solution changed from colorless to yellow. Then, 0.01 g of modified SiO_2NWs was dissolved into 60 mL water. After ultrasonication at 323 K for 1 h, the suspensions were mixed with different volumes of AgNPs and 18 mL 0.1 mg mL^{-1} of GO (the maximum amount of GO combined with SiO_2NWs which was found by the experiment). After that, it was stirred for 2 h. Subsequently, the mixture was centrifuged at 4000 r min^{-1} for 5 min, washed with water for 5 times. The precipitates were re-dispersed in 100 mL of water and reduced by excess $NaBH_4$. Finally, the composites were dried at 333 K. The added amount of AgNPs by different volumes (1, 2, 3, 5, 8, 10 mL) were 0.89, 1.77, 2.64, 4.32, 6.74, 8.28 wt%, respectively. The number of added AgNPs volumes was used to name the different AgNPs/SiO_2NWs/RGO-X Nanocomposites as the X.

2.3 Characterization

The crystalline phases of composites were examined by X-ray diffraction (XRD, Panalytical X'Pert Pro) using Cu K_α radiation ($\lambda = 0.03343$).The composites morphologies were analyzed by scanning electron microscope (SEM, Zeiss Libra, Germany). AgNP size was tested and the microstructure of composite was analyzed by transmission electron microscope (TEM: 200FE, Zeiss Libra, Germany). Identification of the different chemical states of elements was carried out by X-ray photoelectron spectroscopy (XPS, SSX-100). Magnetic hysteresis loops was measured by vibrating sample magnetometer (VSM: BKT-4500Z, China). The nitrogen adsorption–desorption isotherm was measured at 77 Kusing Micromeritics ASAP 2020 adsorption apparatus. The Brunauer–Emmett–Teller (BET) surface area of the sample was evaluated using the nitrogen adsorption isotherms.

2.4 Catalysis

The photocatalytic activity of the AgNPs/SiO_2NWs/RGO nanocomposites were evaluated for 4-nitrophenol reduction by using $NaBH_4$ in the photo reaction apparatus (BL-GHX-V, Bilang Biological Science and Technology Co., Ltd., Xi'an) using a 300 W Xe lamp with an ultraviolet cutoff filter (providing visible light ≥ 400 nm) as the light source to trigger the photocatalytic reaction.

A 10 mL portion of 4-nitrophenol solution (4-NP, 100 mg L^{-1}) and 10 mL of sodium borohydride ($NaBH_4$, 2.7 g L^{-1}) were dropped into quartz test tubes. Next, 10 mg AgNPs/SiO_2NWs/RGO nanocomposite was dropped into the mixture solution, and the reaction was maintained at an appropriate time. The reaction was measured by using an UV–vis spectrophotometer (UV2600A UV–vis spectrophotometer). The composite was recovered by vacuum suction filtration quickly after the photocatalytic reaction.

3 Results and discussion

3.1 Characterization of AgNPs/SiO_2NWs/RGO nanocomposites

In order to study the morphology of RGO and AgNPs on SiO_2NWs surface, the microstructure transformations of SiO_2NWs and the AgNPs/SiO_2NWs/RGO nanocomposites were analyzed by SEM. As shown in Figure S2(a, b), the SEM images of the SiO_2NWs and AgNPs/SiO_2NWs/RGO nanocomposites indicate that RGO nanosheets and AgNPs on SiO_2 NWs surfaces are well-assembled and the integrated material possesses a three-dimensional network structure consisting of mutual cross-linked RGO nanosheets and SiO_2NWs adhered AgNPs. And there is no obvious preferred orientation between RGO sheets and SiO_2NWs, which is in agreement with the existence of strong intermolecular hydrogen bonds. The diameter of SiO_2NWs is almost 50 nm. The three-dimensional network structure indicates that the amino groups modified silica surface is helpful for bonding with graphene oxide and well-distribution of silver nanoparticles. The aminated SiO_2 NWs are negatively charged. Intermolecular hydrogen bonds between amino groups and functional groups (–OH and –COOH groups carboxyl) of GO also exist. The results of FT-IR spectra also proved the presence of hydrogen bonds (see the supporting Information, Figure S3). The electron-deficient AgNPs adhered on the surface of RGO nanosheets and electron-rich amino groups functionalized SiO_2NWs are interacted through electrostatic attraction.

To further investigate the microstructure of RGO and AgNPs on SiO_2NWs surface and the adhesion morphology of AgNPs, the microstructure of AgNPs/SiO_2NWs/RGO nanocomposites with different volumes of AgNPs are determined using transmission electron microscope (Fig. 1). It shows that RGO is coated and cross-linked with SiO_2NWs to form a three-dimensional network structure, and AgNPs are well dispersed and adhered on the surface of RGO and SiO_2NWs. There is no obvious density increase of AgNPs with the increasing of AgNPs content from 5 to 10 mL (Fig. 1a, b). The nanostructure of SiO_2NWsis maintained after chemical treatment. The size distribution of AgNPs is about 10–20 nm (Fig. 1c) and the typical HRTEM image of AgNPs/SiO_2NWs/RGO nanocomposites show the obvious three-dimensional network structure (Fig. 1d). The insets in Fig. 1a, b show the electron diffraction patterns of the samples. It indicated that there are three main growth orientations of the face-centered cubic (fcc) crystalline silver, confirmed by the XRD analysis. Figure 1e, f shows high-resolution TEM (HRTEM) images of Ag nanoparticles. The lattice fringe spacing is calculated as 2.36 Å, corresponding to the (111) crystal plane of Ag (d = 0.236 nm) [23].

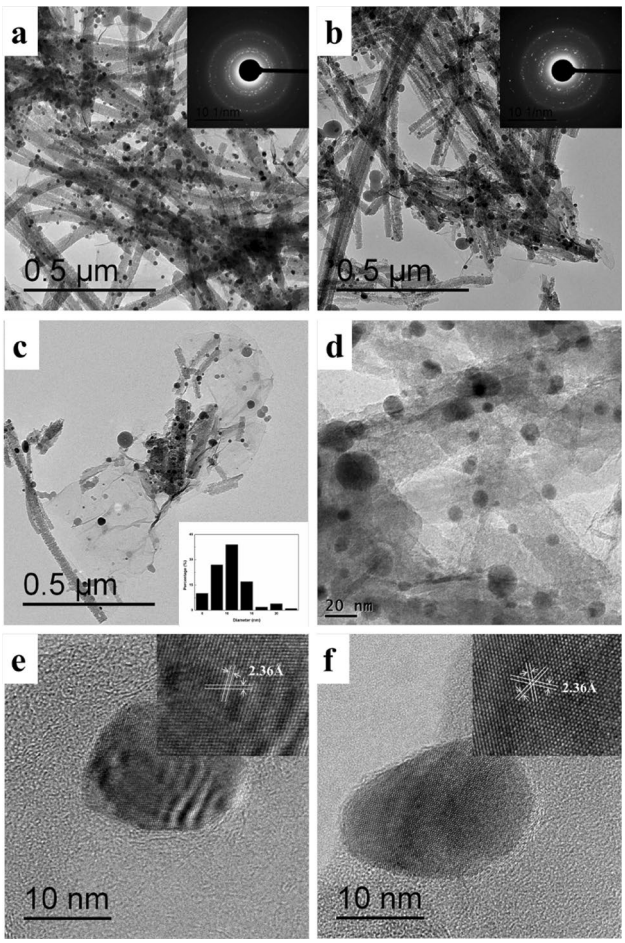

Fig. 1 Typical TEM images (**a**–**c**) and the HRTEM image (**d**) of AgNPs/SiO_2NWs/RGO nanocomposites, **a**, **b** the insets illustrate the electron diffraction patterns of the samples, **c** the inset depicts the size distribution of AgNPs, typical HRTEM images **e**, **f** of Ag nanoparticles, and insets show the growth orientations, ring axis of [111]

XRD patterns of the AgNPs/SiO_2NWs/RGO nanocomposites with different volumes of AgNPs are shown in the Fig. 2. The diffraction peaks with 2θ values of 10.9°, 24.5° and 26.9°, the weak and broad diffraction peak in the region of 2θ = 15°–30° and the diffraction peaks at 38.7°, 65.1° and 77.9° correspond to GO, RGO and G (graphite) [35, 43, 44], SiO_2NWs and the (111), (220), and (311) crystal planes of the face-centered cubic (fcc) crystalline silver, respectively. The diffraction peaks of AgNPs are consistent with the values in standard card (JCPD04-0783). With the increasing of AgNPs, the peak intensity is also increased. The diffraction pattern of SiO_2NWs indicates the amorphous structural feature of SiO_2NWs which are derived from low-order chrysotile. The silica nanowires are not damaged after chemical synthesis. No obvious diffraction peaks of GO and G (graphite) are observed, suggesting the reduction of GO to RGO. Because of the peaks overlap, the diffraction peak of RGO at 25.4° is covered by the peak of SiO_2NWs.

XPS was used for investigating the different valent states of elements of AgNPs/SiO_2NWs/RGO nanocomposite (Fig. 3). Figure 3a shows the representative XPS spectra of the AgNPs/SiO_2NWs/RGO-10 nanocomposite, indicating main chemical compositions are Ag, C, Si, O, N, Fe and Mg elements. With the added amount of AgNPs by different volumes (1, 2, 3, 5, 8, 10 mL), the concentration of Ag in the AgNPs/SiO_2NWs/RGO-X are 0.81, 1.63, 2.03, 3.08, 3.16, 3.29 at.%, respectively. The high-resolution XPS spectra of Ag3d show that the peaks at about 368.4 and 374.4 eV (that transferred to high binding energy with 0.2 eV) are attributed to Ag3$d_{5/2}$ and Ag3$d_{3/2}$, respectively (Fig. 3b). The high-resolution XPS spectra of O1*s* shows that the peaks at about 530.8, 533.3 (that transferred to high binding energy with 0.3, 0.4 eV, respectively) and 532.5 eV are attributed to O1*s* in –O–H, –O and SiO_2, respectively (Fig. 3c). As the stronger ionic character of the countercation is, the lower the binding energies of the framework elements are [45]. In the case of the AgNPs/SiO_2NWs/RGO nanocomposite the valence electron of O in RGO would be shifted toward the H in –O–H and the C in RGO. In addition, the nonpolar nature of RGO made it more difficult to eject a core electron from O in RGO. Therefore, the binding energy of O1*s* in RGO is observed at higher binding energy. The main peak for RGO at 284.6 eV (C=C) in the C1*s* region suggested the formation of grapheme (Fig. 3d). Furthermore, the main peak for SiO_2 at 102.7 eV (Si–O–Si) in the Si2*p* region suggested that the chemical bond of SiO_2 is retained after chemical treatment, and the peak for –NH_2

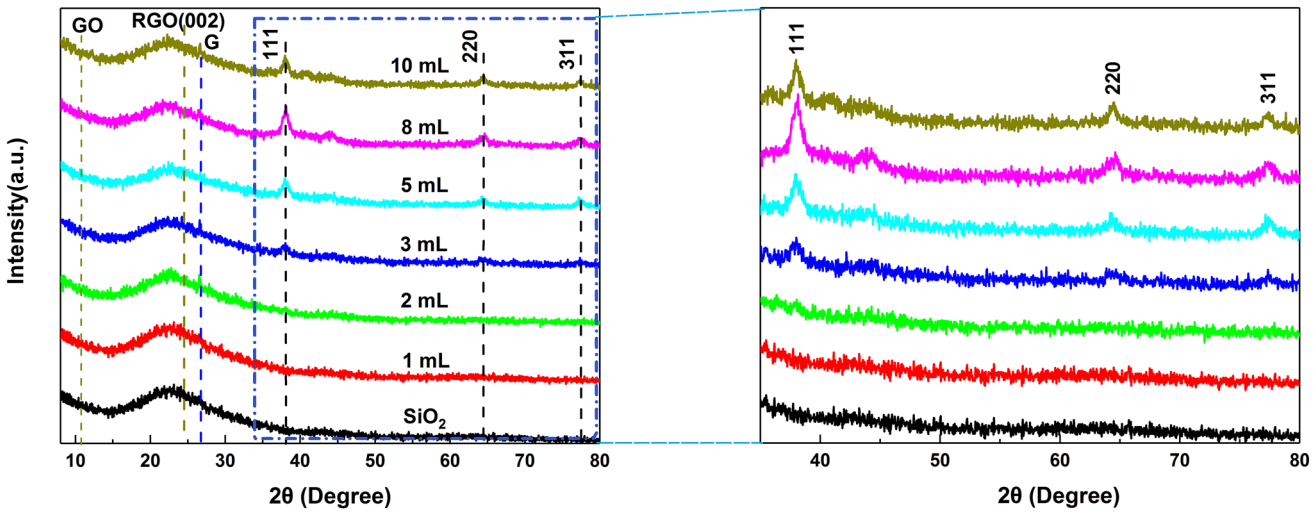

Fig. 2 XRD patterns of AgNPs/SiO_2NWs/RGO nanocomposites with different volumes of AgNPs (1–10 mL). Marked cyan peaks are attributed to standard card (JCPDF 04-0783)

at 400.2, 402.1 eV in the N1*s* region suggested the existence of intermolecular hydrogen bonds (Fig. 3e, f). Since silicon dioxide nanowires were prepared using Chrysotile ($Mg_6[Si_4O_{10}](OH)_6$), the Mg1*s* signal is also presented in the XPS spectra. Finally, the existence of Fe2*p* signal might be caused by the associated mineral of Chrysotile.

Owing to the presence of Fe, magnetic hysteresis loops of the SiO_2NWs and AgNPs/SiO_2NWs/RGO nanocomposites with different volumes of AgNPs (0, 1, 5, 10 mL) are shown in Fig. 4. The SiO_2NWs, SiO_2–NH_2NWs and AgNPs/SiO_2NWs/RGO nanocomposites are the soft magnetic materials. The change of magnetization intensity could be due to the loss of Fe during chemical treatment (the amination with γ-APS). The loss of Fe during the amination mainly comes from the removal of impurities in silica nanowires prepared from natural materials. Because the area surrounded by hysteresis loop is proportional to the energy loss of a complete cycle of magnetization. The addition of RGO and AgNPs did not change the energy loss obviously compared with the SiO_2NWs (Fig. 4a). The concentration of AgNPs had no effect on coercive force (Fig. 4b).

3.2 Catalytic reduction of 4-nitrophenol

Figure 5 shows the UV–vis diffuse reflectance spectra of the five different AgNPs/SiO_2NWs/RGO composites and the pristine SiO_2 nanowires. All the samples exhibit good light absorption in the visible and ultraviolet regions. However, after decoration with AgNPs, each spectrum of AgNPs/SiO_2NWs/RGO shows a localized surface plasm on resonance (LSPR) band with a maximum centered at ca. 400 nm. The presence of a minimum at ca. 320 nm can be also observed, characterizing the inter-band transition of metals that damps the plasm on oscillation in this spectral region. With the increase of silver volume, the intensity of the absorption peak is increased indicating the enhanced LSPR. This behavior is due to two different factors: firstly, the AgNPs immobilized on the SiO_2NWs and RGO mutually enhanced each other's polarizability; secondly, the increasing of charge transfer from the Ag nanoparticles to the RGO sheet. Therefore, the surface plasm on resonance is also enhanced greatly. The AgNPs/SiO_2NWs/RGO-10 exhibits the maximum intensity of the absorption peak.

The reduction of 4-nitrophenol (4-NP) is one of the model reactions for appraising the catalytic activity of noble metal nanoparticle [6, 26]. So the photo-catalytic reduction of nitroaromatic compounds is chosen as a test reaction to investigate the photo-catalytic activity of as-prepared AgNPs/SiO_2NWs/RGO nanocomposite. In fact, the absorption peak of 4-NP solutions is at 317 nm under non-alkaline conditions. The peak is red-shifted to 400 nm because of the formation of 4-nitrophenolate ion after being treated by $NaBH_4$ (see the supporting Information, Figure S5). The color of the 4-NP solutions changes from light-yellow to yellow-grown at the same time.

Figure 6 shows the results of the catalytic reduction of 4-NP. Figure 6a displays the UV–Vis absorption spectra during the catalytic reduction of 4-NP by AgNPs/SiO_2NWs/RGO-10 nanocomposites. After the addition of the AgNPs/SiO_2NWs/RGO-10 nanocomposites, a new peak at 295 nm appears, and which is attributed to the formation of 4-aminophenol. As the reaction time goes by, the successive decreasing of adsorption intensity at 400 nm and that of increasing at 295 nm indicate the nitro compound is

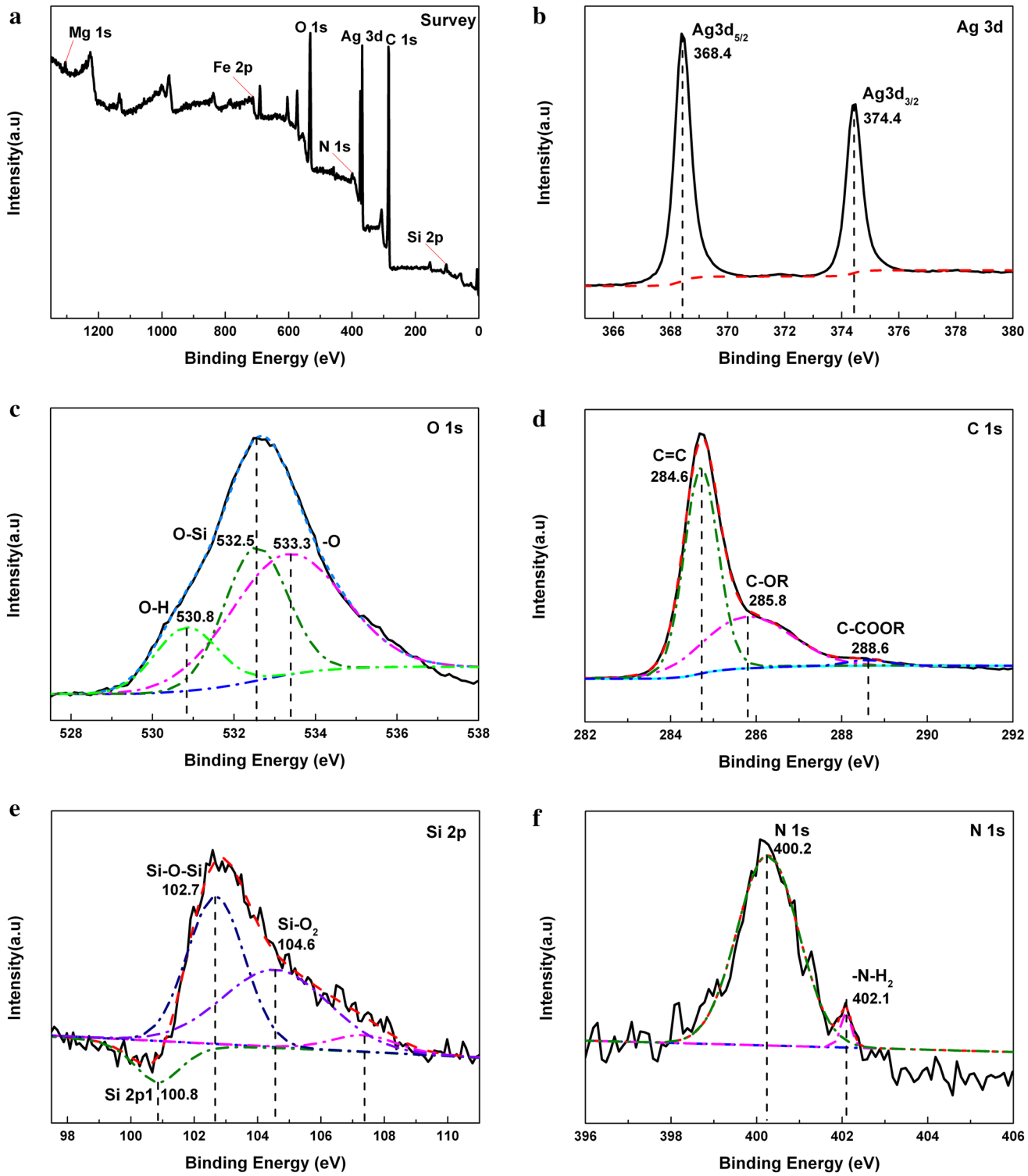

Fig. 3 The XPS spectra of AgNPs/SiO_2NWs/RGO nanocomposites. **a** Survey spectrum; **b** Ag 3*d*; **c** O 1*s*; **d** C 1*s*; **e** Si 2*p*; **f** N 1*s*

gradually transformed into aminophenol, and the nitration could be successfully reduced. Among the different AgNPs/SiO_2NWs/RGO nanocomposites, the catalytic efficiency of AgNPs/SiO_2NWs/RGO-10 is the best (see the supporting Information, Figure S6a–e). By increasing the exposure time, the absorption peak of 4-NP at 400 nm

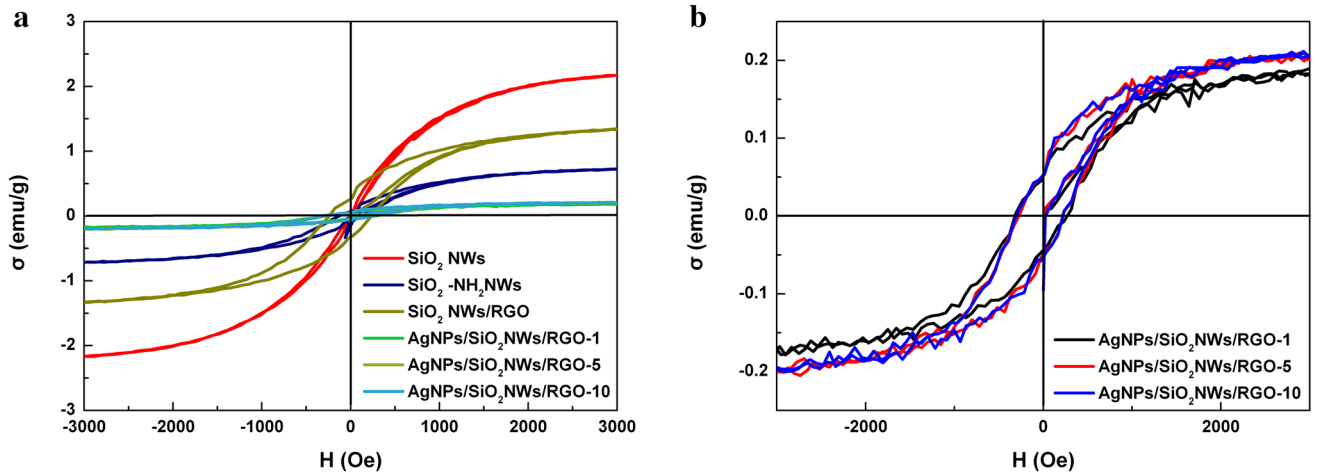

Fig. 4 Magnetic hysteresis loops of the SiO_2NWs and AgNPs/SiO_2NWs/RGO nanocomposites with different volumes of AgNPs (0, 1, 5, 10 mL)

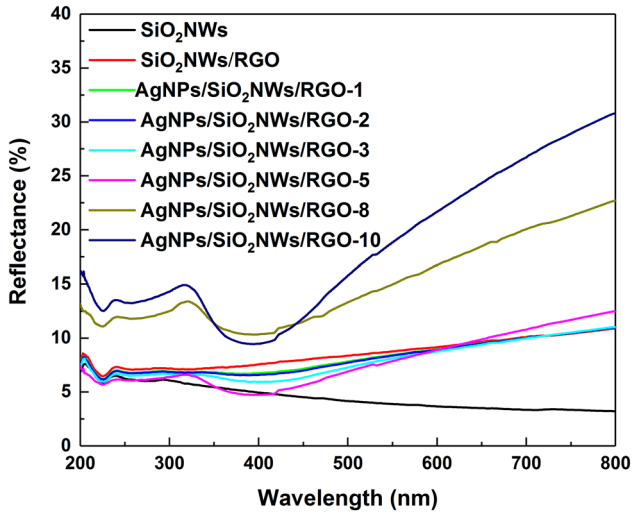

Fig. 5 UV–Vis diffuse reflectance spectra of the SiO_2NWs and AgNPs/SiO_2NWs/RGO nanocomposites with different volumes of AgNPs (0, 1, 2, 3, 5, 8, 10 mL)

diminishes quickly, and which is completely disappeared after about 10 min, suggesting the complete photocatalytic reduction of 4-NP. The AgNPs/SiO_2NWs/RGO nanocomposites exhibit the excellent catalytic efficiency under visible light. Due to the electron-deficient AgNPs played as electron acceptor during the formation of 4-AP, the catalytic activity is increased with the increasing of AgNPs concentration. For comparison, four contrast tests are conducted with the mixture of 4-NP, reducing agent $NaBH_4$, the pristine SiO_2NWs, the RGO modified SiO_2NWs (SiO_2NWs/RGO) under visible light and AgNPs/SiO_2NWs/RGO-10 in dark. The result is shown in the supporting Information Figure S6f. It also shows that the 4-NP concentration decrease of contrast tests should be rather to the adsorption process than the catalytic activity. The SiO_2 NWs and RGO have almost 35% 4-NP absorption in total. The results of nitrogen adsorption–desorption isotherm of SiO_2NWs and AgNPs/SiO_2NWs/RGO nanocomposites support the multilayer adsorption and capillary condensation adsorption mechanisms. The calculated BET surface areas of SiO_2 NWs, AgNPs/SiO_2NWs/RGO-5 and AgNPs/SiO_2NWs/RGO-10 are 151, 205, 200 $m^2\ g^{-1}$, respectively. Large specific surface are confirms of their excellent catalytic activities (see the supporting Information, Figure S7).

The repeatability test was used to investigate the stability of the photochemical catalytic properties of AgNPs/SiO_2NWs/RGO nanocomposites, and the results show that the photocatalytic activity of AgNPs/SiO_2NWs/RGO-10 is outstanding among all kinds of AgNPs/SiO_2NWs/RGO nanocomposites prepared in the current reaction system (Fig. 6c). The high activity after undergoing four catalysis cycles suggesting the composite's good recyclability. After recycling, the structure and morphology of the AgNPs/SiO_2NWs/RGO catalyst is stable, and the three-dimensional network structure is remain exist (see the supporting Information, Figure S8). The catalytic reduction is accompanied by the rapid color change (see the supporting Information, Figure S4). As the hydrophilic surface of the SiO_2 nanowires became hydrophobic after wrapped with RGO [21], the hydrophobic AgNPs/SiO_2NWs/RGO nanocomposites make it easily to be recycled, forming film via filtration process. The kinetics of decomposition can be understood according to physical chemistry principles. The results shown in Fig. 6 imply that the previous catalytic reduction reactions are consistent with the Langmuir–Hinshelwood apparent first order kinetics model because of superfluous $NaBH_4$ used to protect the 4-AP from aerial oxidation compared with 4-NP and catalyst [46].

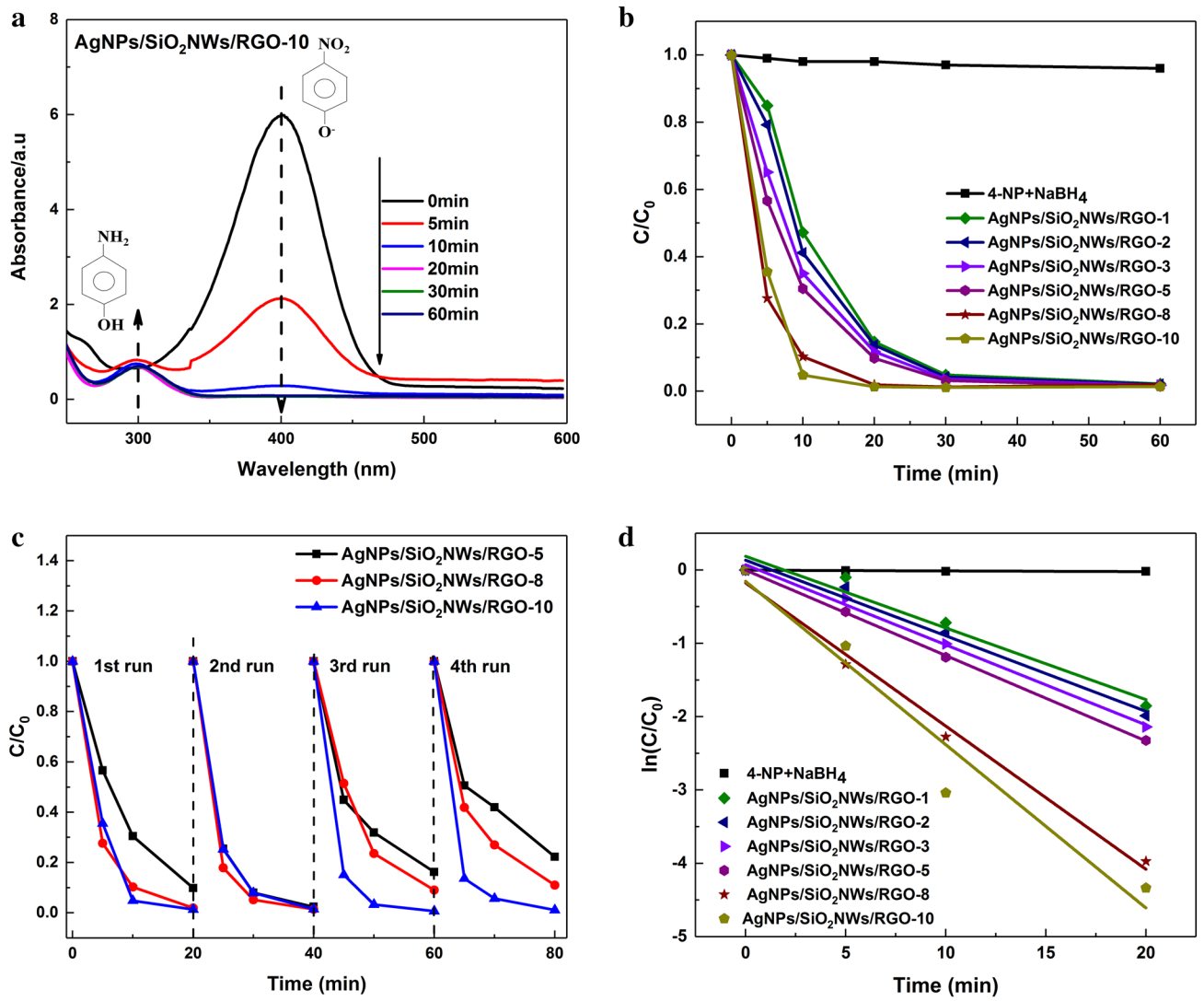

Fig. 6 **a** UV–Vis absorption spectra during the catalytic reduction of 4-NP by AgNPs/SiO_2NWs/RGO-10 nanocomposites, **b** catalytic reduction of 4-NP under visible light irradiation, **c** catalytic reduction of 4-NP with recycled AgNPs/SiO_2NWs/RGO catalysts under visible light irradiation and **d** linearized kinetic curves of 4-NP reduction

Figure 6d shows the linear relationship of $\ln C/C_0$ versus t, and which indicates that the reaction of 4-NP in the presence of AgNPs/SiO_2NWs/RGO nanocomposites followed pseudo-first-order kinetics. It can be observed that AgNPs/SiO_2NWs/RGO exhibits high catalytic activity. While, the samples of AgNPs/SiO_2NWs/RGO-1, 2, 3, 5, 8, 10 result in the reaction rate constants of 1.628, 1.717, 1.820, 1.942, 3.254, and 3.711×10^{-3} s^{-1}, which are some higher than Ag-SiO_2NWs and AgNPs (34.8 mg L^{-1} 4-NP, 2.52×10^{-3} s^{-1}, 2.38×10^{-3} s^{-1}) [12]. This indicates that the catalytic efficiency is significantly enhanced with the increasing silver nanoparticles on the SiO_2NWs and RGO. In addition, our results also imply that AgNPs/SiO_2NWs/RGO nanocomposites would greatly promote the industrial potential application of pristine SiO_2NWs, AgNPs and RGO-SiO_2NWs. Nevertheless, the reaction rate constants are lower than Ag-RGO (10 mg L^{-1} 4-NP, 6.49×10^{-3} s^{-1}) [43]. Although the constant of Ag-RGO is much higher, there is no actual comparability because of the lacked Ag concentration in the paper.

All above analyze show that the insulator SiO_2NWs provide the framework and form the stable three-dimensional network structure with RGO. The adhered AgNPs have the photocatalytic activity, the graphene facilities make the charge separation of the photocatalyst, and the maximum load of GO combined with SiO_2NWs is found to be 18 wt%. Moderate graphene and Ag NPs load lead to the increased

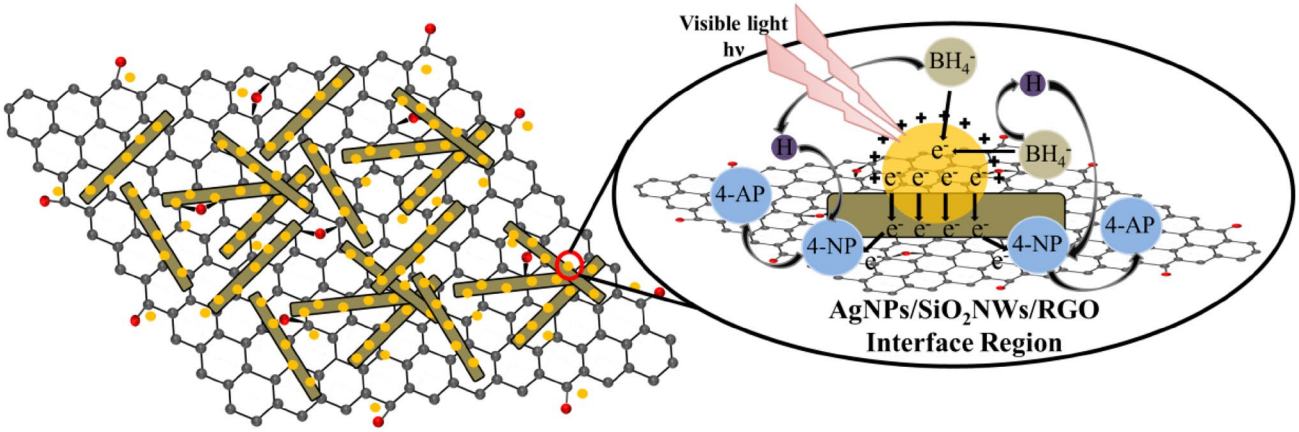

Scheme 2 Possible mechanism of the 4-NP catalytic reduction by the AgNPs/SiO_2NWs/RGO nanocomposites

photocatalytic activity because of the increase of the available surface area for 4-NP adsorption.

3.3 Catalytic mechanism

It has been shown the reduction of 4-NP to 4-AP by $NaBH_4$ is carried out on the surface of AgNPs [18]. According to current theory about the catalytic reduction of 4-NP by AgNPs, electron transfer occurs from BH_4^- to 4-NP. The atomic hydrogen formed from the hydride attacks the 4-NP to produce 4-AP through the adsorption of the reactant onto the Ag catalyst surface. The catalytic efficiency is highly dependent on the large surface area of AgNPs [1, 6, 47]. Previous studies showed that the hydrophilic supports were superior to hydrophobic supports for the catalytic reaction [3, 7]. Therefore, we conclude that the excellent catalytic activity of hydrophobic AgNPs/SiO_2NWs/RGO nanocomposites may be originated from: (1) Its large specific surface area and the easy availability of Ag/SiO_2NWs/RGO interface, which are beneficial to make effective contact between the reactants and relative uniform adhesion and distribution of AgNPs, provide a large amount of active sites, resulting the high catalytic activity. (2) It is served exceptionally as electron acceptor and mediator due to its high carrier mobility [48]. Ag nanoparticles adhered on the surface of RGO and SiO_2NWs could absorb the visible light irradiation by the LSPR effect in which electrons transported from Ag to RGO increase the photocatalytic activity under visible light. RGO efficiently suppresses the charge recombination and improves the charge separation efficiency to enhance the photocatalytic activity. (3) The abundant –OH groups on silica nanowires surface, the oxygen-containing groups of RGO and the π-electron conjugated structure between RGO and SiO_2NWs also play important roles in enhancing the capturing and adsorption of BH_4^- and 4-NP molecules in the reaction region. (4) RGO sheets have high adsorption capacity for 4-NP via π–π stacking interactions [26]. As a result, high concentration of 4-NP is present near the Ag nanoparticles on RGO and SiO_2NWs, leading to better contact between them; the electron transfer from RGO to Ag nanoparticles increases the local electron density, improving the electrons uptake by 4-NP molecules (Scheme 2).

4 Conclusion

In summary, we reported a novel and scalable preparation procedures of AgNPs/SiO_2NWs/RGO nanocomposites with three-dimensional network structure. It was synthesized by using SiO_2NWs prepared from Chrysotile and homemade GO as the suitable holder to combine with AgNPs under the strong hydrogen-bonding and electrostatic adsorption between SiO_2NWs, GO nanosheets and AgNPs. The SiO_2NWs provide the framework and form the stable three-dimensional network structure with RGO. The photocatalytic activity of the AgNPs/SiO_2NWs/RGO was evaluated for 4-nitrophenol reduction by using $NaBH_4$. The composites exhibited high catalytic activity because the nearly mono-dispersed AgNPs were adhered on the surface of SiO_2NWs and RGO, allowing effective active contact and electron transfer between the reactants and catalysis of the reaction. In particular, the as-prepared AgNPs/SiO_2NWs/RGO nanocomposites with 10 mL AgNPs (AgNPs/SiO_2NWs/RGO-10) exhibited excellent catalytic activity. Significantly, these AgNPs/SiO_2NWs/RGO nanocomposites exhibit the superior stability and can be easily reused with a little decline of the catalytic activity due to SiO_2 nanowires natural mineral frameworks with large amounts of active sites and the hydrophobic surface and soft magnetic property of AgNPs/SiO_2NWs/RGO

materials. These nanocomposites show the great prospect for the 4-NP reduction in practice and are promising for wide applications in visible light catalytic reaction.

Funding This study was funded by the Open Foundation of Joint Laboratory for Extreme Conditions Matter Properties, Southwest University of Science and Technology and Research Center of Laser Fusion, CAEP (14tdjk02); the Open Foundation of Nuclear waste and environmental safety National defense key discipline laboratory (15kffk07); Basic Scientific Research Key Project (JCKY2016208B012).

Compliance with ethical standards

Conflict of interest The authors declare that they have no conflict of interest.

References

1. Chi Y, Tu J, Wang M, Li X, Zhao Z (2014) One-pot synthesis of ordered mesoporous silver nanoparticle/carbon composites for catalytic reduction of 4-nitrophenol. J Colloid Interface Sci 423:54–59. https://doi.org/10.1016/j.jcis.2014.02.029
2. Wang M, Fu J, Huang D, Zhang C, Xu Q (2013) Silver nanoparticles-decorated polyphosphazene nanotubes: synthesis and applications. Nanoscale 5(17):7913–7919. https://doi.org/10.1039/c3nr00010a
3. Jianwei Zheng HL, Zheng Xinlei, Duan Xinping, Yuan Youzhu (2013) Highly efficient mesostructured Ag_SBA-15 catalysts for the chemoselective synthesis of methyl glycolate by dimethyl oxalate hydrogenation. Catal Commun 40:129–133. https://doi.org/10.1016/j.catcom.2013.06.022
4. Gao Y, Ding X, Zheng Z, Cheng X, Peng Y (2007) Template-free method to prepare polymer nanocapsules embedded with noble metal nanoparticles. Chem Commun 36:3720–3722. https://doi.org/10.1039/b706490j
5. Chiou JR, Lai BH, Hsu KC, Chen DH (2013) One-pot green synthesis of silver/iron oxide composite nanoparticles for 4-nitrophenol reduction. J Hazard Mater 248–249:394–400. https://doi.org/10.1016/j.jhazmat.2013.01.030
6. Zhang P, Shao C, Zhang Z, Zhang M, Mu J, Guo Z, Liu Y (2011) In situ assembly of well-dispersed Ag nanoparticles (AgNPs) on electrospun carbon nanofibers (CNFs) for catalytic reduction of 4-nitrophenol. Nanoscale 3(8):3357–3363. https://doi.org/10.1039/c1nr10405e
7. Naik B, Hazra S, Prasad VS, Ghosh NN (2011) Synthesis of Ag nanoparticles within the pores of SBA-15: an efficient catalyst for reduction of 4-nitrophenol. Catal Commun 12(12):1104–1108. https://doi.org/10.1016/j.catcom.2011.03.028
8. Wang C, Zhang Z, Yang G, Chen Q, Yin Y, Jin M (2016) Creation of controllable high-density defects in silver nanowires for enhanced catalytic property. Nano Lett. https://doi.org/10.1021/acs.nanolett.6b02317
9. Kang J, Li Y, Chen Y, Wang A, Yue B, Qu Y, Zhao Y, Chu H (2015) Core–shell Ag@SiO_2 nanoparticles of different silica shell thicknesses: preparation and their effects on photoluminescence of lanthanide complexes. Mater Res Bull 71:116–121. https://doi.org/10.1016/j.materresbull.2015.07.017
10. Li Z, Jia L, Li Y, He T, Li X-M (2015) Ammonia-free preparation of Ag@SiO_2 core/shell nanoparticles. Appl Surf Sci 345:122–126. https://doi.org/10.1016/j.apsusc.2015.03.159
11. Shi Y, Zhang X-L, Feng G, Chen X, Lu Z-H (2015) Ag–SiO_2 nanocomposites with plum-pudding structure as catalyst for hydrogenation of 4-nitrophenol. Ceram Int 41(10):14660–14667. https://doi.org/10.1016/j.ceramint.2015.07.188
12. Zhang H, Duan T, Zhu W, Yao W-T (2015) Natural chrysotile-based nanowires decorated with monodispersed Ag nanoparticles as a highly active and reusable hydrogenation catalyst. J Phys Chem C 119(37):21465–21472. https://doi.org/10.1021/acs.jpcc.5b05450
13. Liang M, Su R, Qi W, Yu Y, Wang L, He Z (2013) Synthesis of well-dispersed Ag nanoparticles on eggshell membrane for catalytic reduction of 4-nitrophenol. J Mater Sci 49(4):1639–1647. https://doi.org/10.1007/s10853-013-7847-y
14. Kang H, Yim J, Jeong S, Yang J-K, Kyeong S, Jeon S-J, Kim J, Eom KD, Lee H, Kim H-I, Jeong DH, Kim J-H, Lee Y-S (2013) Polymer-mediated formation and assembly of silver nanoparticles on silica nanospheres for sensitive surface-enhanced Raman scattering detection. ACS Appl Mater Interfaces 5(24):12804–12810. https://doi.org/10.1021/am404435d
15. Dong Z, Le X, Li X, Zhang W, Dong C, Ma J (2014) Silver nanoparticles immobilized on fibrous nano-silica as highly efficient and recyclable heterogeneous catalyst for reduction of 4-nitrophenol and 2-nitroaniline. Appl Catal B 158–159:129–135. https://doi.org/10.1016/j.apcatb.2014.04.015
16. Stefanie Wunder FP, Yan Lu, Mei Yu, Ballauf Matthias (2010) Kinetic analysis of catalytic reduction of 4-nitrophenol by metallic nanoparticles immobilized in spherical polyelectrolyte brushes. J Phys Chem C 114:8814–8820
17. Gao Y, Zhao S, Zhang G, Deng L, Li J, Sun R, Li L, Wong C-P (2015) In situ assembly of dispersed Ag nanoparticles on hierarchically porous organosilica microspheres for controllable reduction of 4-nitrophenol. J Mater Sci 50(9):3399–3408. https://doi.org/10.1007/s10853-015-8898-z
18. Zhang Z, Shao C, Sun Y, Mu J, Zhang M, Zhang P, Guo Z, Liang P, Wang C, Liu Y (2012) Tubular nanocomposite catalysts based on size-controlled and highly dispersed silver nanoparticles assembled on electrospun silicananotubes for catalytic reduction of 4-nitrophenol. J Mater Chem 22(4):1387–1395. https://doi.org/10.1039/c1jm13421c
19. Long S, Li L, Guo H, Yang W, Lu F (2012) Preparation of stable core–shell dye adsorbent Ag-coated silica nanospheres as a highly active surfaced-enhanced Raman scattering substrate for detection of Rhodamine 6G. Dyes Pigm 95(3):473–477. https://doi.org/10.1016/j.dyepig.2012.05.023
20. Liu K, Zhu B, Feng Q, Wang Q, Duan T, Ou L, Zhang G, Lu Y (2013) Adsorption of Cu(II) ions from aqueous solutions on modified chrysotile: thermodynamic and kinetic studies. Appl Clay Sci 80–81:38–45. https://doi.org/10.1016/j.clay.2013.05.014
21. Yang K, Chen B, Zhu L (2015) Graphene-coated materials using silica particles as a framework for highly efficient removal of aromatic pollutants in water. Sci Rep 5:11641. https://doi.org/10.1038/srep11641
22. Liu K, Feng Q, Yang Y, Zhang G, Ou L, Lu Y (2007) Preparation and characterization of amorphous silica nanowires from natural chrysotile. J Non-Cryst Solids 353(16–17):1534–1539. https://doi.org/10.1016/j.jnoncrysol.2007.01.033
23. Pasricha R, Gupta S, Srivastava AK (2009) A facile and novel synthesis of Ag–graphene-based nanocomposites. Small 5(20):2253–2259. https://doi.org/10.1002/smll.200900726
24. Yang Z, Qi C, Zheng X, Zheng J (2015) Facile synthesis of silver nanoparticle-decorated graphene oxide nanocomposites and their application for electrochemical sensing. New J Chem 39(12):9358–9362. https://doi.org/10.1039/c5nj01621e
25. Zahed B, Hosseini-Monfared H (2015) A comparative study of silver–graphene oxide nanocomposites as a recyclable catalyst for the aerobic oxidation of benzyl alcohol: support effect.

Appl Surf Sci 328:536–547. https://doi.org/10.1016/j.apsusc.2014.12.078
26. Al Nafiey A, Addad A, Sieber B, Chastanet G, Barras A, Szunerits S, Boukherroub R (2017) Reduced graphene oxide decorated with Co_3O_4 nanoparticles (rGO-Co_3O_4) nanocomposite: a reusable catalyst for highly efficient reduction of 4-nitrophenol, and Cr(VI) and dye removal from aqueous solutions. Chem Eng J 322:375–384. https://doi.org/10.1016/j.cej.2017.04.039
27. Chakraborty K, Chakrabarty S, Pal T, Ghosh S (2017) Synergistic effect of zinc selenide-reduced graphene oxide towards enhanced solar light-responsive photocurrent generation and photocatalytic 4-nitrophenol degradation. New J Chem 41(11):4662–4671. https://doi.org/10.1039/c6nj04022e
28. Ikhsan NI, Rameshkumar P, Huang NM (2016) Controlled synthesis of reduced graphene oxide supported silver nanoparticles for selective and sensitive electrochemical detection of 4-nitrophenol. Electrochim Acta 192:392–399. https://doi.org/10.1016/j.electacta.2016.02.005
29. Jeffery AA, Rao SR, Rajamathi M (2017) Preparation of MoS_2-reduced graphene oxide (rGO) hybrid paper for catalytic applications by simple exfoliation-costacking. Carbon 112:8–16. https://doi.org/10.1016/j.carbon.2016.11.001
30. Kumar Sahoo P, Panigrahy B, Thakur D, Bahadur D (2017) Ice-templating synthesis of macroporous noble metal/3D-graphene nanocomposites: their fluorescence lifetimes and catalytic study. New J Chem 41(16):7861–7869. https://doi.org/10.1039/c7nj00128b
31. Liu L, Chen R, Liu W, Wu J, Gao D (2016) Catalytic reduction of 4-nitrophenol over Ni–Pd nanodimers supported on nitrogen-doped reduced graphene oxide. J Hazard Mater 320:96–104. https://doi.org/10.1016/j.jhazmat.2016.08.019
32. Meng N, Cheng J, Zhou Y, Nie W, Chen P (2017) Green synthesis of layered 1T-MoS_2/reduced graphene oxide nanocomposite with excellent catalytic performances for 4-nitrophenol reduction. Appl Surf Sci 396:310–318. https://doi.org/10.1016/j.apsusc.2016.10.136
33. Peng J, Weng J (2015) One-pot solution-phase preparation of a MoS_2/graphene oxide hybrid. Carbon 94:568–576. https://doi.org/10.1016/j.carbon.2015.07.035
34. Sahoo PK, Aepuru R, Panda HS, Bahadur D (2015) Ice-templated synthesis of multifunctional three dimensional graphene/noble metal nanocomposites and their mechanical, electrical, catalytic, and electromagnetic shielding properties. Sci Rep 5:17726. https://doi.org/10.1038/srep17726
35. Vilian ATE, Choe SR, Giribabu K, Jang SC, Roh C, Huh YS, Han YK (2017) Pd nanospheres decorated reduced graphene oxide with multi-functions: highly efficient catalytic reduction and ultrasensitive sensing of hazardous 4-nitrophenol pollutant. J Hazard Mater 333:54–62. https://doi.org/10.1016/j.jhazmat.2017.03.015
36. Xia J, He G, Zhang L, Sun X, Wang X (2016) Hydrogenation of nitrophenols catalyzed by carbon black-supported nickel nanoparticles under mild conditions. Appl Catal B 180:408–415. https://doi.org/10.1016/j.apcatb.2015.06.043
37. Yang L, Wang X-z, Liu Y, Yu Z-f, Liang J-j, Chen B-b, Shi C, Tian S, Li X, Qiu J-s (2017) Monolayer MoS_2 anchored on reduced graphene oxide nanosheets for efficient hydrodesulfurization. Appl Catal B 200:211–221. https://doi.org/10.1016/j.apcatb.2016.07.006
38. Ye W, Yu J, Zhou Y, Gao D, Wang D, Wang C, Xue D (2016) Green synthesis of Pt–Au dendrimer-like nanoparticles supported on polydopamine-functionalized graphene and their high performance toward 4-nitrophenol reduction. Appl Catal B 181:371–378. https://doi.org/10.1016/j.apcatb.2015.08.013
39. Zhang X-F, Zhu X-Y, Feng J-J, Wang A-J (2018) Solvothermal synthesis of N-doped graphene supported PtCo nanodendrites with highly catalytic activity for 4-nitrophenol reduction. Appl Surf Sci 428:798–808. https://doi.org/10.1016/j.apsusc.2017.09.200
40. Lu W, Luo Y, Chang G, Sun X (2011) Synthesis of functional SiO_2-coated graphene oxide nanosheets decorated with Ag nanoparticles for H_2O_2 and glucose detection. Biosens Bioelectron 26(12):4791–4797. https://doi.org/10.1016/j.bios.2011.06.008
41. Yin D, Liu B, Zhang L, Wu M (2012) Preparation of a novel core–shell Ag–graphene@SiO_2 nanocomposite for fluorescence enhancement. J Biomed Nanotechnol 8(3):458–464. https://doi.org/10.1166/jbn.2012.1394
42. Hummers WS, Offeman RE, Hummers WS, Offeman RE (1958) Preparation of graphitic oxide. J Am Chem Soc 80(6):1339
43. Meng N, Zhang S, Zhou Y, Nie W, Chen P (2015) Novel synthesis of silver/reduced graphene oxide nanocomposite and its high catalytic activity towards hydrogenation of 4-nitrophenol. RSC Adv 5(87):70968–70971. https://doi.org/10.1039/c5ra13574e
44. Titelman GI, Gelman V, Bron S, Khalfin RL, Cohen Y, Bianco-Peled H (2005) Characteristics and microstructure of aqueous colloidal dispersions of graphite oxide. Carbon 43(3):641–649. https://doi.org/10.1016/j.carbon.2004.10.035
45. Dorota A, Pawlak MI, Oku Masaoki, Shimamura Kiyoshi, Fukuda Tsuguo (2002) Interpretation of XPS O (1*s*) in mixed oxides proved on mixed perovskite crystals. J Phys Chem B 106:504–507
46. Yu Mei YL, Polzer Frank, Ballauff Matthias (2007) Catalytic activity of palladium nanoparticles encapsulated in spherical polyelectrolyte brushes and core–shell microgels. Chem Mater 19:1062–1069
47. Hajfathalian M, Gilroy KD, Yaghoubzade A, Sundar A, Tan T, Hughes RA, Neretina S (2015) Photocatalytic enhancements to the reduction of 4-nitrophenol by resonantly excited triangular gold–copper nanostructures. J Phys Chem C 119(30):17308–17315. https://doi.org/10.1021/acs.jpcc.5b04618
48. Jafari Z, Mokhtarian N, Hosseinzadeh G, Farhadian M, Faghihi A, Shojaie F (2016) Ag/TiO_2/freeze-dried graphene nanocomposite as a high performance photocatalyst under visible light irradiation. J Energy Chem 25(3):393–402. https://doi.org/10.1016/j.jechem.2016.01.013